International Conference on Applied Energy 2019
Aug 12-15, 2019, Västerås, Sweden
Paper ID: 292

INVESTIGATIONS OF WATER DISTRIBUTION IN DIFFERENT FLOW CHANNEL OF PEM FUEL CELL VIA MICROFOCUS X-RAY TOMOGRAPHY

Yiqi Liang, Chasen Tongsh , Xu Xie, Zhijun Peng, Kui Jiao*

State Key Laboratory of Engines, Tianjin University, 135 Yaguan Road, Tianjin, 300350, China

*Corresponding author: kjiao@tju.edu.cn; tel: +86-22-87455090; fax: +86-22-27406949

ABSTRACT

In this study, the water distribution in different flow channels of proton exchange membrane (PEM) fuel cell is investigated experimentally using microfocus X-ray tomography. The high-frequency resistance (HFR) and electrochemical impedance spectrum (EIS) are introduced to determine the electrochemical characteristics of a cell with different flow channels. It is found that although the serpentine-serpentine (s-s) flow channel configuration has the best drainage effect, its pumping loss and membrane resistance at low humidity are large. Conversely, the drainage effect of the parallel-parallel (p-p) flow channel is the worst, but its membrane resistance and pumping loss are the lowest. It is indicated that the serpentine-parallel (s-p) flow channel has better drainage capacity and performance than the p-p flow channel as well as lower pumping loss and better membrane hydration than the s-s channel.

Keywords: Visualization; Flow channel; Water content

1. INTRODUCTION

Proton exchange membrane (PEM) fuel cell has received extensive attention due to its high power density, rapid start up and low emissions [1,2]. An important influencing factor on PEM fuel cell performance and durability is water management. On the one hand, the membrane needs proper wetting to reduce the membrane resistance and improve conductivity. On the other hand, water accumulated in the cathode may lead to the increase of mass transfer loss and pumping loss [3].

In previous literature, there exist four main methods for water distribution visualization in fuel cells, including direct visualization, neutron imaging, nuclear magnetic resonance and X-ray imaging [4]. Aslam et al. [5] found that the fuel cell performance and wetted bend ratio increased with the increase of the operating pressure. Nishida et al. [6] pointed out that the hydrophobic coating of the horizontally oriented serpentine channel was the most effective method to prevent water blocking. Yang et al. [7] designed a transparent fuel cell, showing that the surface tension played a more important role than gravitational and air drag forces. Ge et al. [8] proposed that increasing the anode temperature appropriately was an effective method to reduce anode flooding. Weng et al. [9] showed that the membrane will dehydrate and the membrane resistance will increase when the cathode gas is non-humidified because of large stoichiometry. Spernjak et al. [10] proposed that the serpentine channel was able to operate with high liquid water content in the flow field due to the large pressure drop. The flow field could effectively remove water, and there was no channel blockage for a long time. Klages et al. [11] used the neutron technique to study the condensate removal in three different flow channels. Boillat et al. [12] pointed out that the fuel cell voltage tended to decrease when a bigger amount of water was observed at the cathode side. Lee et al. [13] utilized the change of gray level of water in the X-ray images to determine the water distribution between the separator and gas diffusion layer (GDL) quantitatively. Lee et al. [14] compared the behavior of liquid water with/without micro-porous layer (MPL) in the PEM fuel cell. Banerjee et al. [15] showed that the hydration of membrane was affected significantly by the relative humidity (RH) of anode inlet gas. In addition, the change of current density had an insignificant impact on the water content of the membrane.

Although visualization and electrochemical techniques have been used in the study of fuel cells, it is

still rare to use them together for fuel cell analysis. Visualization can more intuitively reflect the results of electrochemical testing. In this study, three kinds of channel assembly methods are compared.

2. EXPERIMENT

2.1 Fuel cell setup

The membrane electrode assembly (MEA) was supplied by the Wuhan WUT New Energy Co., Ltd. It is noted that the serpentine-parallel, called s-p, represents that the serpentine and parallel flow field are inserted in anode and cathode side, respectively, and so do parallel-parallel (p-p) and serpentine-serpentine (s-s). The MEA, graphite bipolar plate, current collector and the stainless end-plate were assembled together in sequence by screw at a torque of 5 Nm. A hole of 30mm×10mm was dug in the center of the graphite bipolar plate, current collector plate and the stainless end-plate to reduce the attenuation of X-rays penetrating the metal layers. The detailed physical parameters are listed in Table 1.

Table 1. Fuel cell parameters.

Parameters	Value
Active area (cm^2)	25
Membrane	Gore WUT-EV
Membrane thickness (μm)	15
Pt loading in the anode (mg cm^{-2})	0.1
Pt loading in the cathode (mg cm^{-2})	0.4
Assembly torque (Nm)	5

The fuel cell testing system could test and record fuel cell operation parameters, including inlet flow, inlet RH, inlet pressure, back pressure, fuel cell voltage, current and power. Two heating strips were placed at the anode and cathode end-plate to heat the fuel cell to the set temperature. The K-type thermocouple was plugged into the graphite bipolar plate, monitoring the cell temperatures during the experiment. Meanwhile, the testing system also included Zahner electrochemical workstation, which was used for measuring high-frequency resistance (HFR) and electrochemical impedance spectrum (EIS).

2.2 X-ray tomography setup

All experiments were carried out using microfocus X-ray tomography equipment. X-rays are generated by the interaction between high-speed electrons and materials. Electrons emitted from the cathode would be focused on a point on the target, called the X-ray focus. The smaller the focus size of the X-ray source, the higher the resolution of the image and the sharper the image.

The visualization experimental device is mainly composed of an X-ray generator and an X-ray detector. Fig 1 shows the schematic diagram of X-ray tomography. The X-ray generator was supplied by the X-ray Worx in Germany. The maximum voltage of the device is 225 kV and the maximum current is 3 mA. In addition, the maximum transmit power and the maximum target power are 350 W and 300 W, respectively. During the experiment, the tube voltage and the tube current of the X-ray generator were 150 kV and 800 μA. The X-ray detector is provided by Varex. The receiver type is amorphous silicon with a panel size of 13 cm×13 cm, pixel matrix of 1024×1024 (1×1), pixel size of 127 μm^2, and the energy ranging from 40 kVp to 160 kVp.

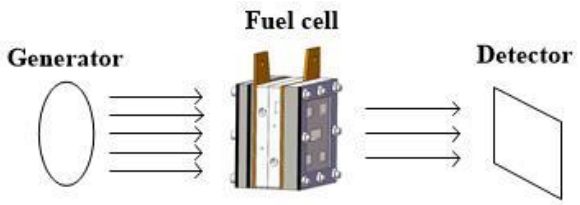

Fig 1. Schematic diagram of X-ray tomography

2.3 Experimental procedures

The MEA was activated by discharging at a constant current density from zero to a maximum power density with incremental steps of 200 mA cm^{-2} every 15 min. Then two currents around the maximum power density were chosen and scanned back and forth three times. Each current remained constant for 45 minutes. After each operation of the fuel cell, 1.0 SLPM nitrogen was used to purge the anode and cathode sides, to dry them. Concurrently, the HFR was tested by the electrochemical workstation. The experiment would start when the HFR reached the desired value before the operation. During the visualization experiment, hydrogen and oxygen (0.5/1.0 SLPM) were supplied to the cell and a constant current of 50 A was applied. The standard experimental protocol is shown in Table 2.

X-ray tomography equipment was used to record the dry flow channel for initial data before the test. During the first three minutes of constant-current operation, the electrochemical workstation was used to test the HFR of the fuel cell. After galvanostatic operating condition for five minutes stably, the EIS was tested and the water in the flow channel was photographed. Due to the uncertainty of the experiment, it is necessary to do more experiments to find the same trend of the picture for comparison.

Table 2. Standard experimental protocol for visualization test.

No.	Step name	Operating conditions	Duration
1	Activation	T_{cell} = 60℃, Variable current densities	4.5 hours
2	Polarization curve	T_{cell} = 60℃, T_{in}=25℃,RH=100%	30 min
3	Purge	T_{cell} = 60℃, $V_{an/ca}$=1/1 SLPM	1 hour
4	Galvanostatic operation	T_{cell} = 60℃, I=50A	15 min
5	Purge	T_{cell} = 60℃, $V_{an/ca}$=1/1 SLPM	1 hour

3. RESULTS AND DISCUSSION

3.1 Effect of water content in the flow channel

Fig 2 shows the results of the visualization experiment from the direction shown in Fig 1. After figure post process, the higher value of a point in the image indicates the higher water content at this point. Specific values can refer to the color chart. Obviously, there is almost no liquid water left in the s-s flow channel while the p-p flow channel is almost fully occupied by liquid water (Fig 2 (a) and (c)). For the s-p case, the amount of liquid water decreased significantly compared with the p-p case. This is because the water removal of the anode flow field has been improved significantly due to high pressure drop in the serpentine flow channel. At the same time, there is a relatively high rate of back diffusion because of the higher content of liquid water in the cathode than the anode. Thus, the drainage capacity of the cathode has also been partially improved.

Fig 3 shows the results taken from the direction perpendicular to the flow field, where the water distribution in anode and cathode flow channel can be observed. It is found that the cathode drainage is significantly improved after the anode flow channel is shifted into the serpentine flow channel.

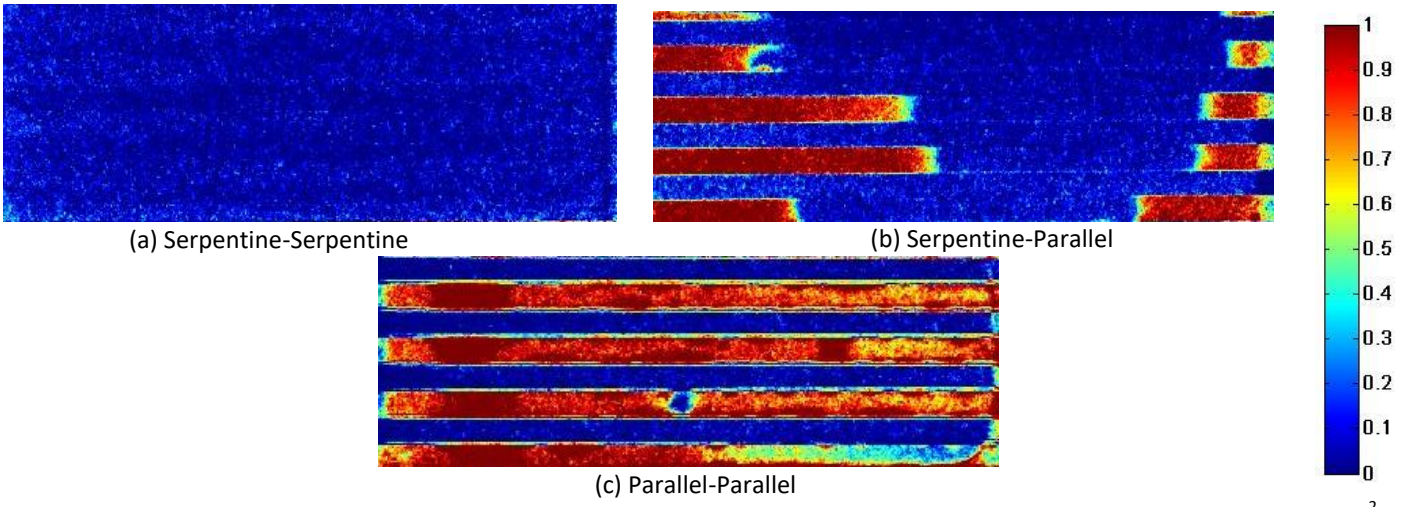

(a) Serpentine-Serpentine

(b) Serpentine-Parallel

(c) Parallel-Parallel

Fig 2. X-ray radiographic images highlighting the appearance of liquid water at various flow field, at a current density of 2 A cm^{-2}.

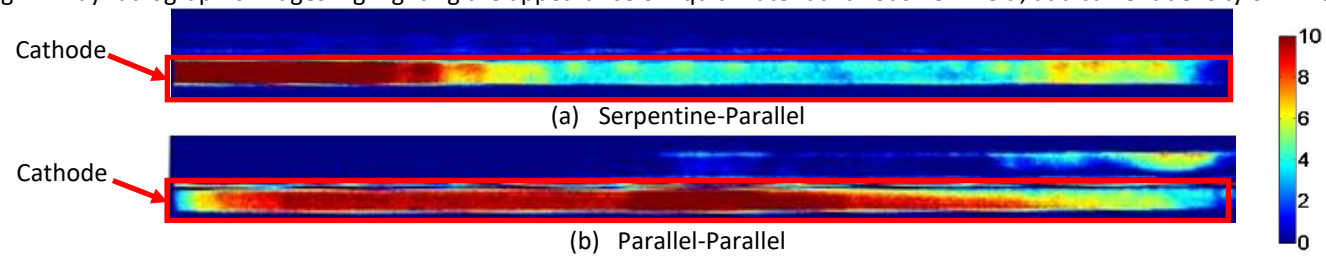

(a) Serpentine-Parallel

(b) Parallel-Parallel

Fig 3. X-ray radiographic images highlighting the distribution of liquid water in anode and cathode at various flow field, at a current density of 2 A cm^{-2}.

3.2 Effect of water content in the membrane

HFR is an experimental tool to measure the ohmic resistance of fuel cells in real time. Typically, the HFR includes ohmic resistance of current collector, flow field, MPL, GDL, contact resistance, membrane resistance, electronic resistance and ionic resistance of

catalyst layer (CL). Since the ionic resistance of membrane and CL will increase with the increase of water content in the unsaturated condition, HFR can reflect the change of water content in the cell [16].

Fig 4 illustrates the HFR test results for different flow fields of 2 A cm^{-2}. The cell of s-s flow field has a higher HFR than that of p-p case. It may because that the s-s flow field has a strong drainage capacity, leading to less water content in the membrane at low humidity. It should be pointed out that the inlet RH is extremely low (16%) so that water in the membrane would be dried easily. That would lead to a larger ohmic resistance, which may cause the folding and fracture of the membrane.

The membrane resistance of s-p case is between the p-p case and s-s case. Since the anode is replaced by a serpentine flow field with better drainage capacity, the liquid water content of anode is largely reduced compared with cathode, promoting the back diffusion and reducing HFR. The water content in the membrane of the s-p flow field is less than that of the p-p flow field due to its better drainage.

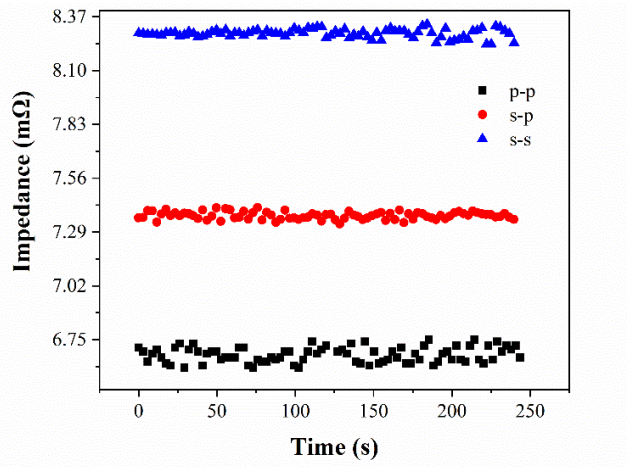

Fig 4. Evolution of HFR of the different flow fields, at a current density of 2 A cm^{-2}

3.3 Effect of electrochemical impedance spectrum and polarization curve

Fig 5 and Fig 6 compare the performances of three different flow fields. After the anode is replaced by the serpentine flow channel, the fuel cell power density is increased by 20% at a current density of 2.75 A cm^{-2}. HFR change is consistent with the conclusion insection3.2. The p-p flow field fuel cell has the largest mass transfer loss (largest second arc), indicating that the water flooding is serious. For the polarization loss, the s-s case has the smallest polarization loss, and that of s-p flow field case is much smaller than the p-p flow field. The s-p flow field has less water in the flow channel than p-p flow field so that the reactant can enter in CL easily. Furthermore, the charge transfer resistance is small because of more reaction sites due to not severe water flooding in CL.

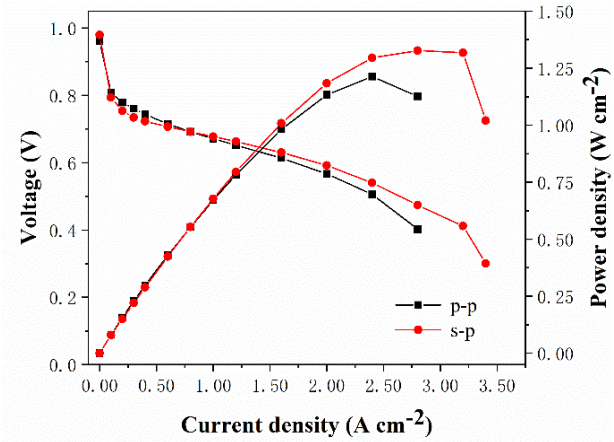

Fig 5. Comparison of the polarization curves of s-p and p-p.

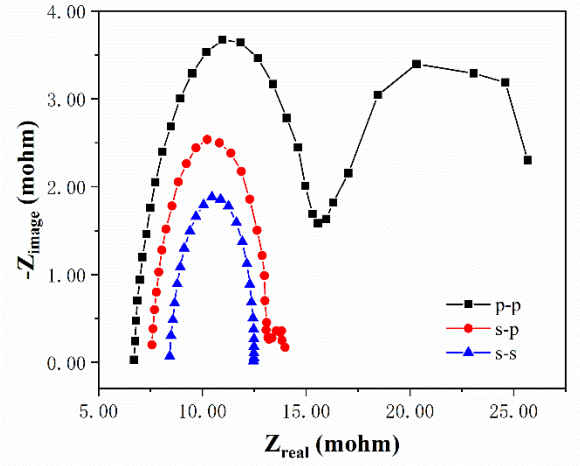

Fig 6. Comparison of EIS of three flow field.

4. CONCLUSION

A microfocus X-ray imaging technique is used to observe the distribution and transport behavior of water in different flow channels in proton exchange membrane (PEM) fuel cell. The high-frequency resistance (HFR) and electrochemical impedance spectrum (EIS) are considered.

It is found the drainage capacity and fuel cell performance of serpentine-parallel flow field is better than that of parallel-parallel flow field. Compared with serpentine-serpentine flow field, serpentine-parallel flow field manages to hydrate the proton exchange membrane under low inlet humidity and thus increases the durability of the membrane and reduces pumping loss. The results in this work can provide further insight

into flow filed optimization in the future PEMFC structure design.

However, there are still some problems in this study. The experimental data was not quantified. In future investigations, it is necessary to consider the quantification of the data.

ACKNOWLEDGEMENT

This research is supported by the National Natural Science Foundation of China for Excellent Young Scholars (Grant No. 51622606) and the Natural Science Foundation for Outstanding Young Scholars of Tianjin (Grant No. 18JCJQJC46700).

REFERENCE

[1] P. Pei and H. Chen, "Main factors affecting the lifetime of Proton Exchange Membrane fuel cells in vehicle applications: A review," *Applied Energy*, vol. 125, pp. 60-75, 2014.

[2] Y. Wang, K. S. Chen, J. Mishler, S. C. Cho, and X. C. Adroher, "A review of polymer electrolyte membrane fuel cells: Technology, applications, and needs on fundamental research," *Applied Energy*, vol. 88, pp. 981-1007, 2011.

[3] Z. Wang, Y. Zeng, S. Sun, Z. Shao, B. Yi. "Improvement of PEMFC water management by employing water transport plate as bipolar plate," *International Journal of Hydrogen Energy*, vol. 42, pp. 21922-21929, 2017.

[4] O.S. Ijaodola, Z. El- Hassan, E. Ogungbemi, F.N. Khatib, Tabbi Wilberforce, James Thompson, A.G. Olabi, "Energy efficiency improvements by investigating the water flooding management on proton exchange membrane fuel cell (PEMFC)," *Energy*, 2019.

[5] R.M. Aslam, D.B. Ingham, M.S. Ismail, K.J. Hughes, L. Ma, M. Pourkashanian, "Simultaneous direct visualization of liquid water in the cathode and anode serpentine flow channels of proton exchange membrane (PEM) fuel cells," *Journal of the Energy Institute*, vol. 91, pp. 1057-1070, 2018.

[6] K. Nishida, R. Taniguchi, Y. Ishizaki, S. Tsushima, S. Hirai, "Impacts of channel wettability and flow direction on liquid water transport in the serpentine flow field of a polymer electrolyte fuel cell," *Journal of Power Sources*, vol. 275, pp. 447-457, 2015.

[7] X. G. Yang, F. Y. Zhang, A. L. Lubawy, C. Y. Wang, "Visualization of Liquid Water Transport in a PEFC," *Electrochemical and Solid-State Letters*, vol 7, pp. A408-A411, 2004.

[8] S. Ge, C. Wang, "Liquid Water Formation and Transport in the PEFC Anode," *Journal of the Electrochemical Society*, vol. 154, pp. B998-B1005, 2007.

[9] F. Weng, A. Su, C. Hsu, C. Lee, "Study of water-flooding behavior in cathode channel of a transparent proton-exchange membrane fuel cell," Journal of Power Sources, vol. 157, pp. 674-680, 2006.

[10] D. Spernjak, A. K. Prasad, S. G. Advani, "Experimental investigation of liquid water formation and transport in a transparent single-serpentine PEM fuel cell," *Journal of Power Sources*, vol. 170, pp. 334-344, 2007.

[11] M. Klages, S. Enz, H. Markötter, I. Manke, N. Kardjilov, J. Scholta, "Investigations on dynamic water transport characteristics in flow field channels using neutron imaging techniques," *Journal of Power Sources*, vol. 239, pp. 596-603, 2013.

[12] P. Boillat, D. Kramer, B.C. Seyfang, G. Frei, E. Lehmann, G.G. Scherer, A. Wokaun, Y. Ichikawa, Y. Tasaki, K. Shinohara, "In situ observation of the water distribution across a PEFC using high resolution neutron radiography," *Electrochemistry Communications*, vol. 10, pp. 546-550, 2008.

[13] S. Lee, N. Lim, S. Kim, G. Park, C. Kim, "X-ray imaging of water distribution in a polymer electrolyte fuel cell," *Journal of Power Sources*, vol. 185, pp. 867-870, 2008.

[14] J. Lee, J. Hinebaugh, A. Bazylak, "Synchrotron X-ray radiographic investigations of liquid water transport behavior in a PEMFC with MPL-coated GDLs," *Journal of Power Sources*, vol. 227, pp. 123-130, 2013.

[15] R. Banerjee, N. Ge, C. Han, J. Lee, M.G. George, H. Liu, D. Muirhead, P. Shrestha, A. Bazylak, "Identifying in operando changes in membrane hydration in polymer electrolyte membrane fuel cells using synchrotron X-ray radiography," International Journal of Hydrogen Energy, vol. 43, pp. 9757-9769, 2018.

[16] S. Basu. "Recent Trends in Fuel Cell Science and Technology," Springer: New York, USA, 2007; pp. 32-35.